AFOSR-TR- 81-0331

LEVEL II

12

PRELIMINARY RESULTS OF A STUDY OF UNSTEADY AIRFOIL SURFACE PRESSURES AND TURBULENT BOUNDARY LAYERS

AD A097560

MASSACHUSETTS INSTITUTE OF TECHNOLOGY
AEROPHYSICS LABORATORY

by

Peter F. Lorber
and Eugene E. Covert

Massachusetts Institute of Technology
Department of Aeronautics and Astronautics
Cambridge, Ma 02139

DTIC
ELECTE
APR 8 1981
C

FINAL REPORT

TR 210

December, 1980

Distribution
Unlimited

DTIC FILE COPY

AFOSR Contract No. F49620-79-C-0226

814 7 055

Approved for public release;
distribution unlimited.

AIR FORCE [illegible] OF SCIENTIFIC RESEARCH (AFSC)
NOTICE [illegible]
This [illegible] approved [illegible] reviewed and is
Distribu[illegible] unlimited.
A. D. [illegible]
Technical Information Officer

Unclassified

SECURITY CLASSIFICATION OF THIS PAGE (When Data Entered)

REPORT DOCUMENTATION PAGE	READ INSTRUCTIONS BEFORE COMPLETING FORM
1. REPORT NUMBER: AFOSR-TR-81-0331	2. GOVT ACCESSION NO. AD-A097 560
	3. RECIPIENT'S CATALOG NUMBER
4. TITLE (and Subtitle): PRELIMINARY RESULTS OF A STUDY OF UNSTEADY AIRFOIL SURFACE PRESSURES AND TURBULENT BOUNDARY LAYERS	5. TYPE OF REPORT & PERIOD COVERED: FINAL 9/1/79 - 9/30/80
	6. PERFORMING ORG. REPORT NUMBER: TR-210
7. AUTHOR(s): PETER F. LORBER, EUGENE E. COVERT	8. CONTRACT OR GRANT NUMBER(s): F49620-79-C-0226
9. PERFORMING ORGANIZATION NAME AND ADDRESS: MASSACHUSETTS INSTITUTE OF TECHNOLOGY, AEROPHYSICS LABORATORY, CAMBRIDGE, MASSACHUSETTS 02139	10. PROGRAM ELEMENT, PROJECT, TASK AREA & WORK UNIT NUMBERS: 61102F 2307/A2
11. CONTROLLING OFFICE NAME AND ADDRESS: AIR FORCE OFFICE OF SCIENTIFIC RESEARCH, BUILDING #410, BOLLING AFB, D.C. 20332	12. REPORT DATE: DECEMBER, 1980
	13. NUMBER OF PAGES: 37
14. MONITORING AGENCY NAME & ADDRESS (if different from Controlling Office)	15. SECURITY CLASS. (of this report): UNCLASSIFIED
	15a. DECLASSIFICATION/DOWNGRADING SCHEDULE

16. DISTRIBUTION STATEMENT (of this Report)

Approved for public release;
distribution unlimited.

17. DISTRIBUTION STATEMENT (of the abstract entered in Block 20, if different from Report)

18. SUPPLEMENTARY NOTES

19. KEY WORDS (Continue on reverse side if necessary and identify by block number)

GROUND TESTING
WIND TUNNELS
UNSTEADY FLOW
UNSTEADY BOUNDARY LAYER

20. ABSTRACT (Continue on reverse side if necessary and identify by block number)

It is shown that aerodynamic interference can produce unsteady flow over a fixed airfoil up to reduced frequencies of 6.4 . The resulting pressure distributions are well behaved, repeatable and, within limits, predictable. Further it is shown that the resulting boundary layer velocity profile can be measured with the same precision as in the steady flow.

DD FORM 1 JAN 73 1473 EDITION OF 1 NOV 65 IS OBSOLETE

Unclassified

SECURITY CLASSIFICATION OF THIS PAGE (When Data Entered)

TECHNICAL ACCOMPLISHMENTS

Introduction

This paper provides a summary of the procedures and recent results of a project whose fundamental goal is the experimental study of unsteady turbulent boundary layers in adverse pressure gradients. Such boundary layers are important in many aeronautical applications, including gas turbines and compressors, helicopter rotors, and maneuvering aircraft. Presently a two-dimensional, low Mach number flow over a NACA-0012 airfoil section provides the test conditions. A rotating elliptical cylinder located behind and beneath the airfoil trailing edge is the source of an unsteady perturbation of variable frequency. At present operating speeds of 9 to 30 mps, perturbation reduced frequency ranges from 0.5 to 6.3. Two-dimensionality of the experiment is preserved by sealing gaps between the airfoil and sidewalls, and by spreading the sidewalls to compensate for boundary layer growth on the sidewalls and maintain uniform static pressure.

The advantage of this technique is that the airfoil surface remains stationary, allowing hot wire velocity measurements in the boundary layer to be readily obtained. The disadvantage is that the disturbance amplitude is fixed for a given frequency, and ellipse location, and is not uniform along the airfoil chord, being of much greater amplitude at the trailing edge.

Previous experimentation in this project involved measuring steady state parameters. Kanevsky[1] measured the pressure distribution produced by circular cylinders of varied diameter and position relative to the airfoil and compared this to the pressure disturbance created by the elliptical cylinder and to that expected for a cambered airfoil at angle of attack.

Cervisi[2] measured pressure and boundary layer velocity profiles for different steady orientations of the elliptical cylinder. This defined the quasi-steady behavior of the wing-cylinder system.

Induced Upwash Measurements

Research over the past year has concentrated on taking initial unsteady measurements. This research is reported in References 3 and 4. First the upwash induced along the airfoil chord by the rotating elliptical cylinder was measured. An X-hot wire probe was used to determine vertical and horizontal velocity components. Figures 1 and 2 show the test configuration and its relation to the tunnel cross section. The wind tunnel being used is the Wright Brothers Wind Tunnel which has an 8x10 foot elliptical cross section.

The instrumentation used for these initial tests was all analog in nature, as seen in Fig. 3. Each hot wire was operated using constant temperature anemometry circuits. The outputs were linearized and passed through a sum/difference amplifier to obtain vertical and horizontal velocity components. A trigger signal was produced by a photo-electric pulser on each revolution of the elliptical cylinder shaft. This trigger was used to synchronize real time oscilloscope displays, FM data tape recording, and the waveform eductor. This device performed phase-locked averaging by dividing the periodic waveform into 100 segments, and time-averaging each segment. Thus, for example, if the cylinder period was ΔT, the 20th step in the average was an average of the input voltage at time equal 20/100 times ΔT after the trigger pulse over a selected number of cycles, typically of order 100. The phase-locked average tends to eliminate all random noise and turbulence components of frequency not equal to a multiple

of the cylinder frequency. This process was primarily useful for determining the amplitude and phase of the primary harmonic as well as showing the shape of the average waveform.

Figure 4 shows the mean induced angle plotted against distance from the position of airfoil leading edge, for a free stream velocity of 30 mps and reduced frequency $K = \frac{\omega c}{2U_\infty}$ varying between 1 and 5. Note the increased angle near the trailing edge. The increase with frequency is a result of increasing cylinder circulation. Figure 5 shows the amplitude of the fundamental harmonic against distance at reduced frequency equal to 1 for varied air speeds. This plot demonstrates that, while minor variations exist in induced angle of attack, reduced frequency seems to be the most important parameter.

Airfoil Surface Pressures

The second series of measurements were of the unsteady pressures on the airfoil surface. The upper and lower surfaces were each fitted with 17 pressure taps along the center line. The taps for each surface were connected to a scanivalve tap selector and capacitive pressure transducer. By comparing the response to a pure acoustic tone of this tap, tubing, yarn, scanivalve, and transducer system to that of the transducer alone, the frequency response was determined to be flat up to 800 Hz with a drop in amplitude to 50% at 1000 Hz. Since the fundamental frequencies considered here range from 5 to 100 Hz this is felt to be satisfactory. Figure 6 shows the tap locations.

Accession For
NTIS CRA&I
DTIC TAB
Unannounced
Justification
By
Distribution/
Availability
Dist Special
A

The instrumentation block diagram for these measurements and for the velocity profile measurements is shown in Figure 7. With the exception of the addition of a spectrum analyzer and averager, the system is the same as that discussed above. Test conditions studied included air speeds of 9,

20, and 30 mps with reduced frequencies of 0.5, 1.0, 1.5, 2.0, 4.0, and 6.3 . Initially the airfoil angle of attack was kept at 0°. The first class of results involve difference pressures. Measured difference pressures were compared to predictions made using Theodorsen's unsteady thin airfoil theory[5] based on the previously measured induced upwash. Figure 8 illustrates a typical comparison for the mean pressure difference. The line is the induced upwash based prediction, while the X's are the pressure data. Figure 9 shows the fluctuating difference pressure amplitude. Qualitative agreement exists, but the measured amplitude is less than the upwash prediction. This difference increases with reduced frequency. Figure 10 shows the phase shift of the fundamental frequency. Agreement is fair over the front 90% of the airfoil, while there is a sharp difference at the trailing edge. Phase shift is defined here as the difference in time between the minimum of the quantity and the minimum obstruction position of the elliptical cylinder. Several possible explanations for these discrepancies exist. The most important being the limitation of the theory to linear, incompressible processes with the product $K M \ll 1$. In other words, the effect of the boundary layer on the unsteady flow is not included in the theory. The presence of a finite thickness, uncusped trailing edge may also contribute to the discrepancy. In this connection Archibald[6], Satyanarayana and Davis[7], and Fleeter[8], have also observed differences between measured unsteady difference pressures and predictions.

The second class of pressure results involve individual surface pressures. Mean surface pressures, as shown in Fig. 11, seemed quite well behaved, largely dependent only on reduced frequency, and then exhibiting only an increasing difference due to the increased cylinder circulation. The fluctuating surface pressures show more interesting behavior. Figure 12 shows the amplitude and Fig. 13 the phase for the fundamental at reduced

frequency 0.5 . These results are qualitatively similar to the behavior expected based on the quasi-steady results. One point of interest is the large jump in phase at the leading edge stagnation point. A major shift in behavior occurs for reduced frequencies of 2 or larger. Figures 14 and 15 show amplitude and phase of the fundamental at reduced frequency 4.0 . The amplitude is somewhat reduced, particularly at the leading edge, but the primary difference is in the phase over the front 20% of the airfoil. Instead of the gradual increase in upper surface phase seen at lower frequencies, a sharp drop occurs. Large phase shifts near the front on unsteady airfoils were also seen by Franke and Henderson[9]. No convincing explanation of this behavior has yet been found.

Two summary plots are shown in Fig. 16 which shows the behavior of the fluctuating pressure coefficient on the upper and lower surface and their difference at X/C = 0.7. The important point to note is the two distinct zones. At low reduced frequencies one type of behavior occurs, namely the pressure coefficient is constant or decreasing, while at high reduced frequencies the pressure coefficient is increasing. This implies that there is a change in the dominant phenomena from the convective processes at low reduced frequencies to smaller scale local unsteady processes at higher reduced frequencies. In contrast to this result, Fig. 17 shows that the RMS pressure coefficient change across the airfloi tends to approach zero at the trailing edge. The nature of the approach seems only weakly dependent upon the reduced frequency. Table I shows the relation of these results to other results in the literature.

Reference	7	8	10	11	12	Present
Airfoil	NACA 64A010	NACA 65 Series	Circular Arc	NACA 0012	NACA 64A010	NACA 0012
Type of Perturbation	Pitching Airfoil	Compressor Rotors	Vorticity Shed From Cylinder	Downstream Shutters	Pitching & Plunging Airfoil	Rotating Elliptical Cylinder
Convected Disturbance	No	Mostly	Yes	No	No	No
Mach Number	0.17	0.03	0.25	0.03	0.5 - 0.8	0.03 - 0.09
Reduced Frequency	0.05 - 1.2	7.5 - 10.1	3.9	0.18 - 0.9	0.026 -0.255	0.5 - 6.4
$k^2M^2/(1-M^2)$	<0.004	0.09	0.67	<0.0007	0.32	0.30
Pressure Tap Locations, X/C	0.4, 0.89 - 0.973	0.90 - 0.97	0.10 - 0.90	0.0 - 0.82	0.3 - 0.94	0.0 - 0.98
ΔC_p(X/C=1) --> ?	0	0 for flat plate in cascade & isolated $\neq$ 0 for cambered cascade	0	0	0	0
Unsteady Difference PPressure & Theory:						
Amplitude	Experiment Less, More Difference for K > 8	Experiment Greater, esp. for Cambered Cascade	Experiment Greater	---	"Good" Agreement for Subsonic	Experiment Less, Differences Increased with K
Phase	Experiment Less, More Difference for K > 8	Fair	Chordwise Variation Greater Than Thoery	---	"Good" Agreement for Subsonic	Fair Away from Trailing Edge

NOTE: Ref. 6 is for blunt trailing edges. Hence it was not listed here.

TABLE 1

SUMMARY OF UNSTEADY AIRFOIL DATA

Boundary Layer Velocity Profiles

The third series of unsteady measurements were airfoil boundary layer velocity profiles. The physical set up is seen in Fig. 18. The hot wire probe may be translated perpendicular to the surface in 0.02 mm or greater increments, with a total travel of 9 cm. Translation is performed using a DC motor, with relative probe position being determined with a linear potentiometer. Since the boundary layer thickness (99% of external mean velocity) is typically 6 mm at 70% of chord and 1.25 cm at 94%, the 6 cm travel allows flexibility in positioning the probe at various chordwise locations and airfoil angles of attack, while keeping probe motion normal to the surface. Some problems have occured in operating within the nearest 0.2 mm from the surface. Vibrations caused by both wind tunnel fluctuations and by the rotating cylinder can cause the hot wire to brush against the surface and break at the joint to its support. The inability to reliably approach the surface has also affected the determination of the position of zero height. It had been hoped to find zero height by the completion of a low current circuit when the probe touched the surface, however not being able to safely get near the surface prevented this. Zero height was operationally determined by extending the linear velocity profile in the laminar sublayer to zero velocity. Heights determined in this manner were consistent to within 0.06 cm for varied profiles at the same location.

Figure 19 shows a mean velocity profile for $K = 2.0$, $X/C=.94$. Mean profiles tended to be relatively insensitive to the unsteady fluctuations. That is, the mean profile for K=1 is very similar to that for K=6.3 for the same chordwise location (and therefore about the same mean pressure gradient).

Figure 20 shows a logarithmic mean velocity profile. Note that the axes are referenced to the external velocity rather than to the friction velocity. This is because methods to estimate the friction velocity from the velocity profile have not given convincing and unambigous results. An unsteady skin friction gauge is being developed to independently find the friction velocity, but it was not available for these tests. The multiplicitive factor in the velocity axis is a streamline curvature correction. This correction is the cause of the downturn in the profile for logarithmic heights above 4, which actually are above the boundary layer.

Figure 21 shows a root-mean-square velocity profile. The RMS velocity includes the fundamental frequency, its harmonics, turbulence, and wind tunnel fan noise. Figure 22 shows the fundamental harmonic amplitude. Note in particular the factor of 2 increases in amplitude perturbation velocity. External amplitudes ranged from 5% of the mean velocity at 95% of chord, reduced frequency 1.0 or less to 0.5% for the 68% of chord, K=6.4 case. The velocity phase shift relative to the external velocity is shown in Fig. 23. Lower frequency cases in general had smaller shifts, of order 5 or 10 degrees, while the high frequency cases were characterized by positive shifts of 15° or higher in the logarithmic region of the mean profile, switching to negative phase near the surface, in the region of highest velocity amplitude.

Future Work

While the above results, produced largely using analog instrumentation are encouraging in that they define the basic characteristics of the wing-rotating cylinder system, future work including the collection of data for non-zero airfoil angles of attack and for additional chordwise boundary

layer measurement locations will require the implimentation of a digital data collection and real-time analysis system. This system will involve triggering the data acquisition using the cylinder shaft pulser, digitizing and storage of unprocessed data, phase-locked averaging of data over many cycles (similar to that previously done using the eductor) Fourier transformation to find the amplitude and phase for arbitrary harmonics, ensemble averaging, and real-time graphics display of selected results to verify equipment operation and to quickly identify new phenomena deserving further study.

Also to be added, as mentioned above, is a wall shear gauge. This will be important both to normalize properly the velocity profile and because wall skin friction is in itself an important aerodynamic parameter.

Future near term research will involve the study of unsteady pressure and boundary layer profiles at non-zero angle of attack, up to static stall and velocity profiles across the wake to attempt to shed light onto the unusual behavior of the phase of the trailing edge difference pressure. Further away are studies of unsteady separation, its correlation to other unsteady boundary layer processes including the evolution of discrete structure within the boundary layer.

REFERENCES

1. Kanevsky, A. R., "Comparison of the Pressure Distribution for Circulation Generated by Angle of Attack with that Generated by Trailing Edge Perturbation," S. M. Thesis, Aeronautics & Astronautics Department, M.I.T., February 1978.

2. Cervisi, R. T., "Turbulent Boundary Layer on an Airfoil in Several Adverse Pressure Gradients," S. M. Thesis, Aeronautics & Astronautics Department, M.I.T., September 1978.

3. Lorber, P. F., "Unsteady Airfoil Pressures Induced by Perturbation of the Trailing Edge Flow," S. M. Thesis, Aeronautics and Astronautics Department, M.I.T., February 1981.

4. Lorber, P. F., and Covert, E. E., "Unsteady Airfoil Pressures Produced by Periodic Aerodynamic Interference," to be submitted to AIAA Journal.

5. Theodorsen, T,, "General Theory of Aerodynamic Instability and the Mechanics of Flutter," NACA Report 496, 1934.

6. Archibald, F. S., "Unsteady Kutta Condition at High Values of the Reduced Frequency Parameter," Journal of Aircraft, Vol. 12, 1975, pp. 545-550.

7. Satyanarayana, B., and Davis, S., "Experimental Studies of Unsteady Trailing Edge Conditions," AIAA Journal, Vol. 16, February 1978, pp. 125-129.

8. Fleeter, S., "Trailing Edge Conditions for Unsteady Flows," AIAA Journal, Vol. 18, May 1980, pp. 497-504.

9. Franke, G. F., and Henderson, R. E., "Unsteady Stator Response to Upstream Rotor Wakes," Journal of Aircraft, Vol. 17, July 1980, pp. 500-508.

10. Commerford, G. L., and Carta, F. O., "Unsteady Aerodynamics Response of a Two-Dimensional Airfoil at High Reduced Frequency," AIAA Journal, Vol. 12, January 1974, pp. 43-48.

11. Saxena, L. S., Fejer, A. A., and Morkovin, M. V., "Features of Unsteady Flows over Airfoils," AGARD CP-227, 1978, pp. 22-1 - 22-11.

12. Davis, S. S. and Malcolm, G. M., "Experiments in Unsteady Transonic Flow," AIAA Paper 79-0769, April 1979.

INTERACTIONS

SPOKEN PAPER AT 54TH SEMI-ANNUAL MEETING

SUPERSONIC TUNNEL ASSOCIATION

9-10 October 1980

NEW DISCOVERIES

The results generated in this contract period include:

1. While surface pressures at the trailing edge are difficult to measure, data up to X/C = 0.98 extrapolates such that the Kutta condition seems to be satisfied up to reduced frequencies of 6.4 . (Note we define the Kutta condition as "The velocity remains finite at the trailing edge". Thus a finite jump in pressure at the trailing edge satisfies the Kutta condition under this definition). The phase lag at the trailing edge is geater than predicted by simple theory.
2. In the Reynolds Number range of .3 to 1.0 x 10^6 and in the MIT Wright Brothers Wind Tunnel the unsteady pressure distribution seems to be well correlated as a function of reduced frequency.
3. Aerodynamic Interference is suitable for producing an unsteady forcing function that will produce a well behaved unsteady boundary layer, as supported by preliminary data.

WRITTEN PUBLICATIONS

Lorber, P. F., and Covert, E. E., "Unsteady Airfoil Pressures Produced by Periodic Aerodynamic Interference," to be submitted to AIAA Journal.

PERSONNEL ASSOCIATED WITH THE PROJECT

Prof. E. E. Covert	Professor of Aeronautics, MIT
Dr. C. W. Haldeman	Associate Director, MIT Aerophysics Laboratory
A. R. Kanevsky	Research Assistant
R. T. Cervisi	Research Assistant
P. F. Lorber	Research Assistant
R. Lee	Research Assistant

DEGREES AWARDED

A. R. Kanevsky	S.M. in Aeronautics, Massachusetss Institute of Technology, February 1978
R. T. Cervisi	S. M. in Aeronautics, Massachusetts Institute of Technology, September 1978
P. F. Lorber	S. M. in Aeronautics, Massachusetts Institute of Technology, February 1981

FIG. 1 CONFIGURATION FOR INDUCED UPWASH TEST

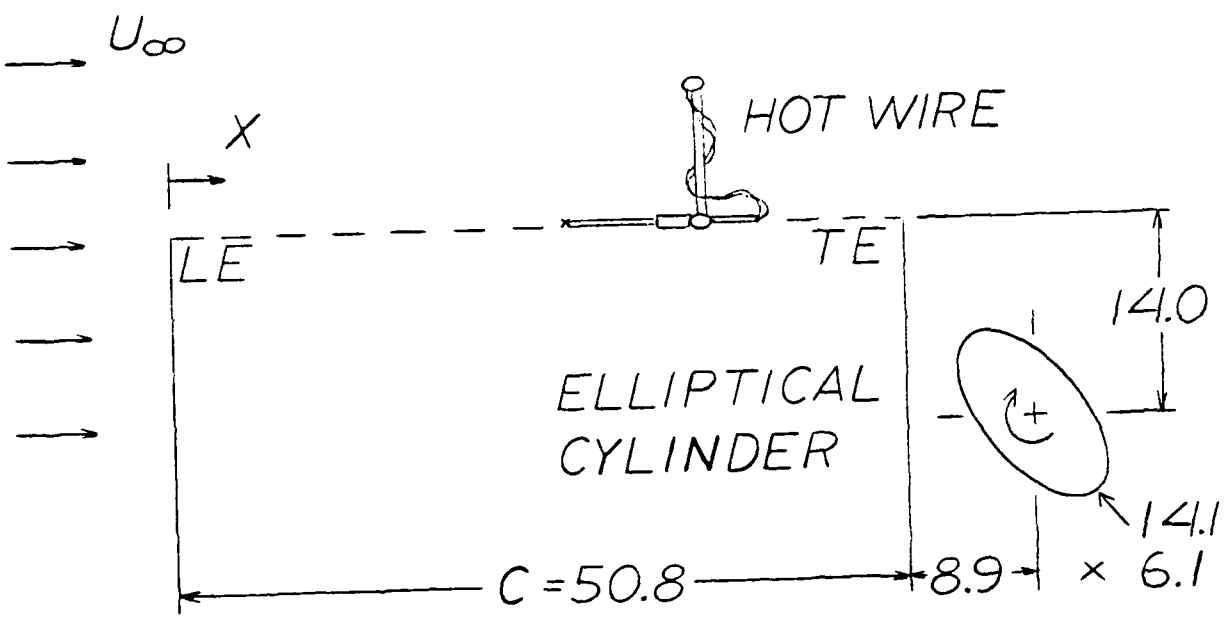

DIMENSIONS IN CM

WIND TUNNEL TEST SECTION
FOR INDUCED UPWASH TEST

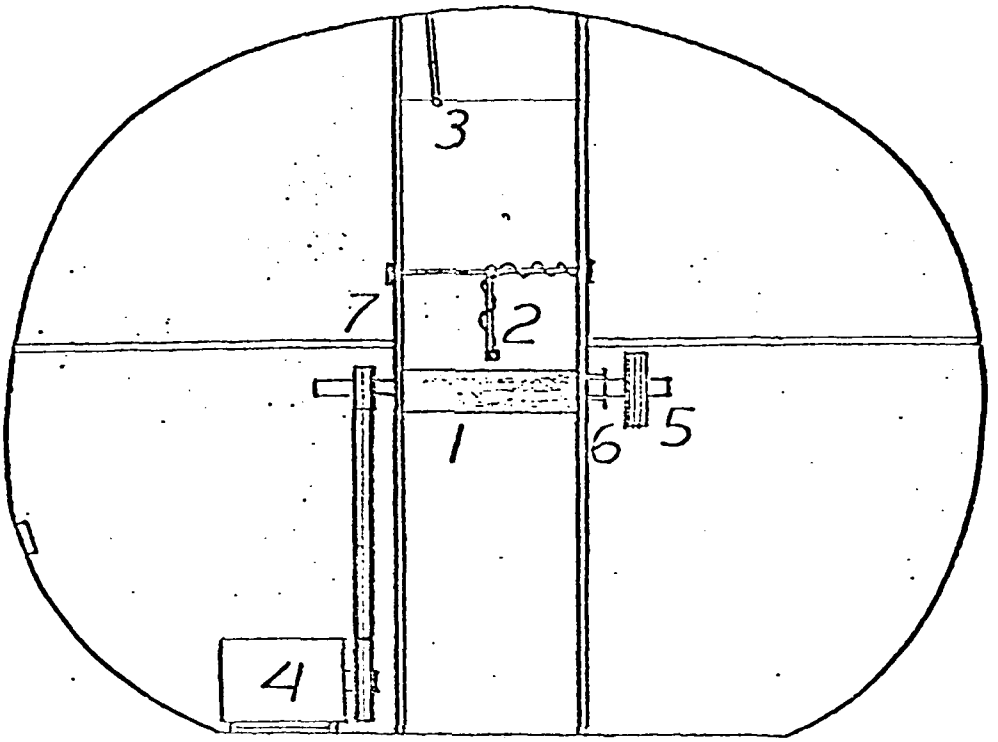

1. ROTATING ELLIPTICAL CYLINDER
2. X HOT WIRE PROBE
3. PITOT STATIC PROBE
4. 2 HP DC MOTOR
5. FLYWHEEL
6. PHOTOELECTRIC PHASE SENSOR
7. SIDEWALLS AND SUPPORTS

FIG. 2

INSTRUMENTATION FOR INDUCED UPWASH MEASUREMENTS

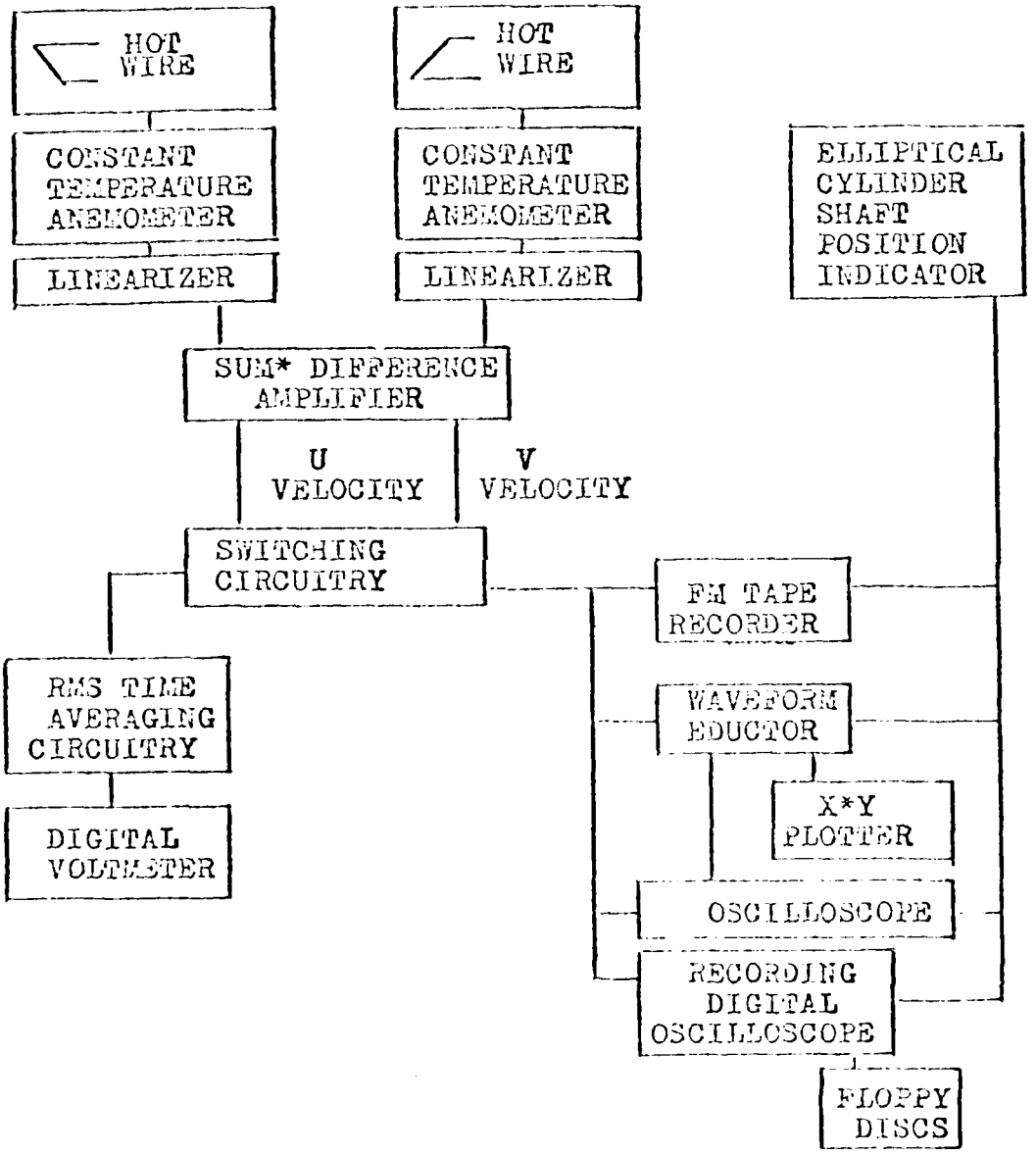

FIG. 3

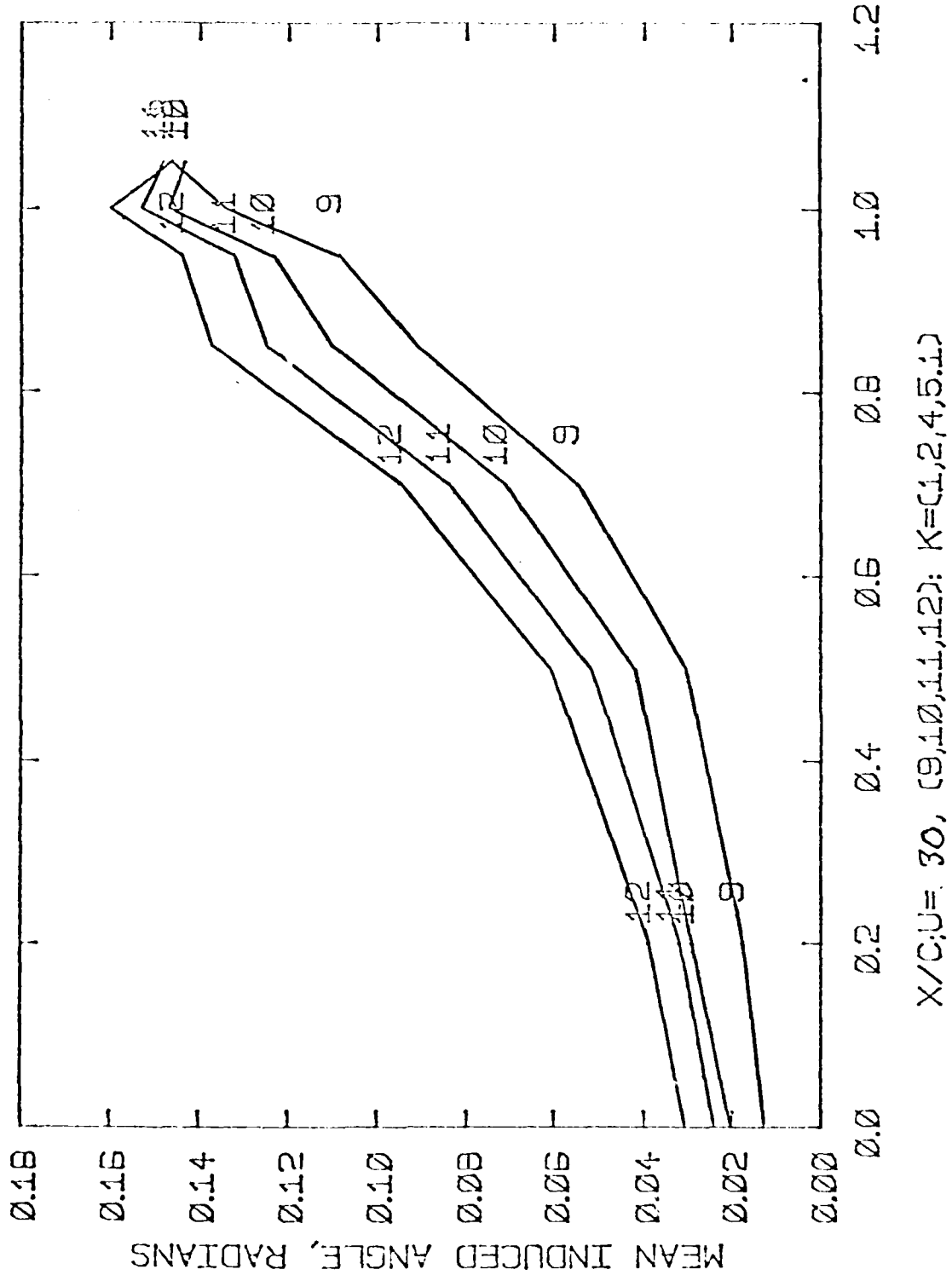
MEAN INDUCED ANGLE, RADIANS
Ø.18
Ø.16
Ø.14
Ø.12
Ø.10
Ø.08
Ø.06
Ø.04
Ø.02
Ø.00
Ø.0
Ø.2
Ø.4
Ø.6
Ø.8
1.0
1.2
X/C;U= 30, (9,10,11,12); K=(1,2,4,5.1)

FIG.4

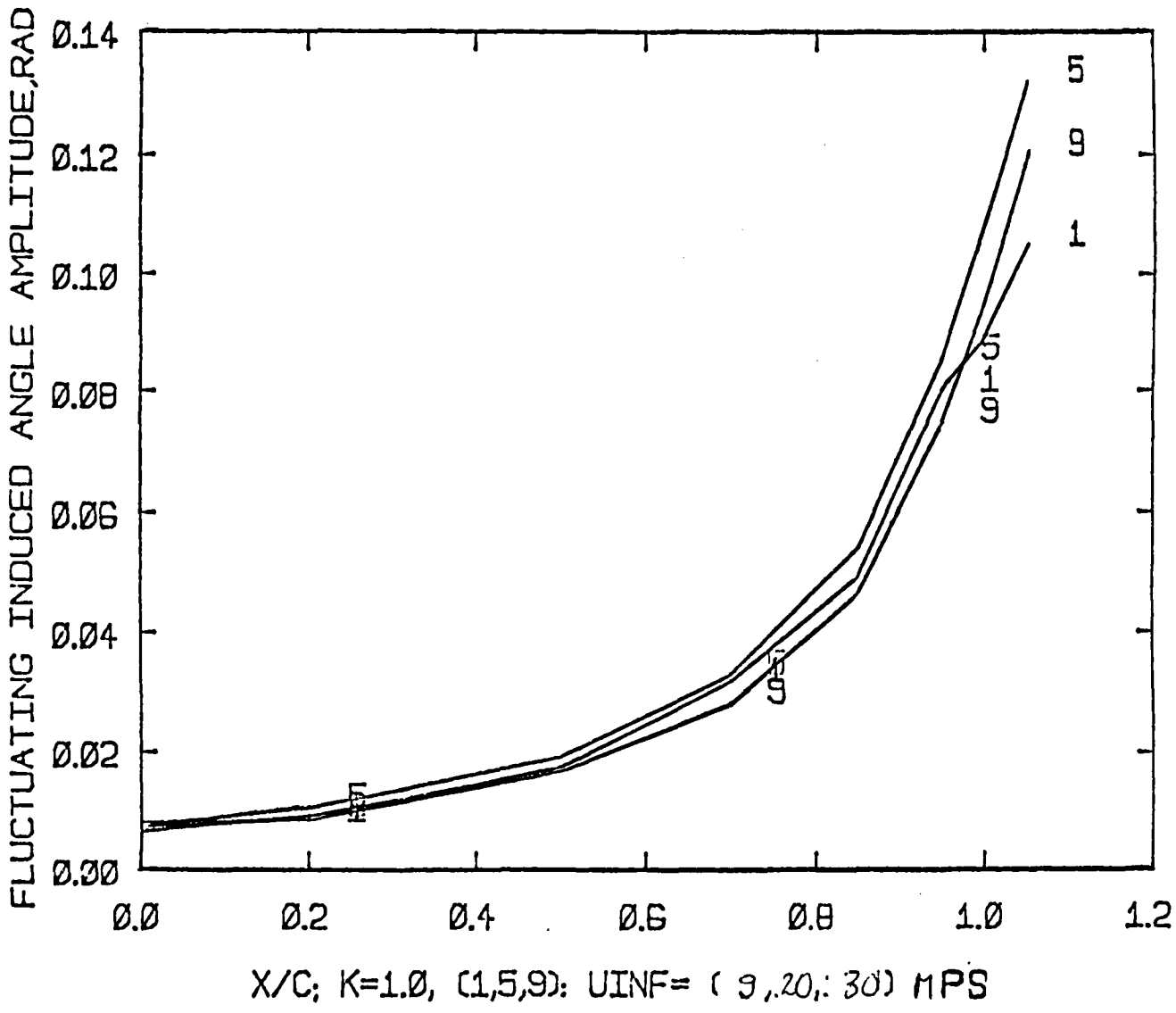
FLUCTUATING INDUCED ANGLE AMPLITUDE,RAD
0.14
0.12
0.10
0.08
0.06
0.04
0.02
0.00
0.0
0.2
0.4
0.6
0.8
1.0
1.2
5
9
1
X/C; K=1.0, (1,5,9): UINF= (9,.20,: 30) MPS

FIG.5

POSITION OF PRESSURE TAPS AND BOUNDARY LAYER VELOCITY MEASUREMENT POINTS

TAP #	POSITION X/C
1	.000
2	.005
3	.025
4	.050
5	.100
6	.150
7	.200
8	.300
9	.400
10	.500
11	.600
12	.700
13	.750
14	.800
15	.850
16	.900
17	.950
18	.980

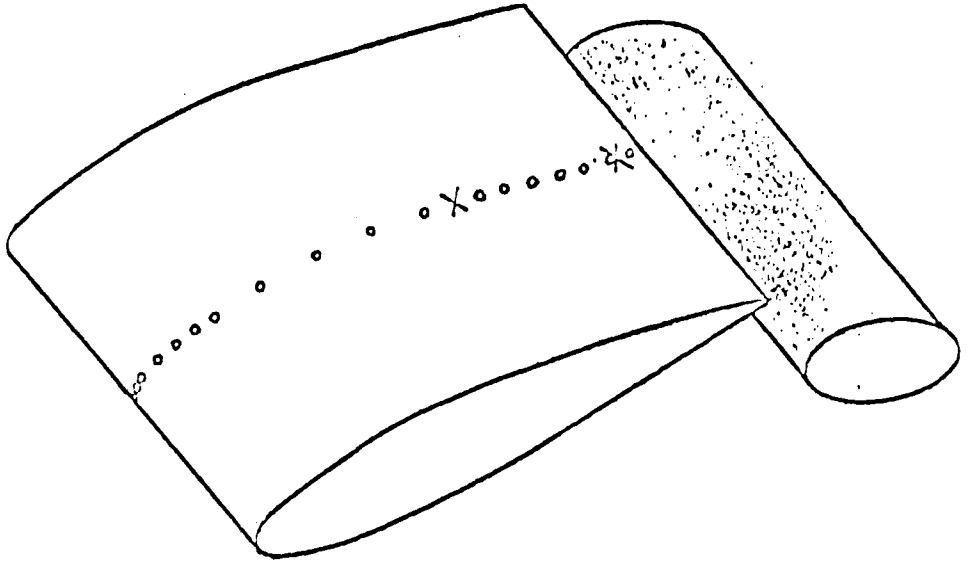

O PRESSURE TAP LOCATION

X VELOCITY PROFILE MEASUREMENT LOCATION, X/C = .6875; .9380.

FIG. 6

PRESSURE AND VELOCITY TEST INSTRUMENTATION

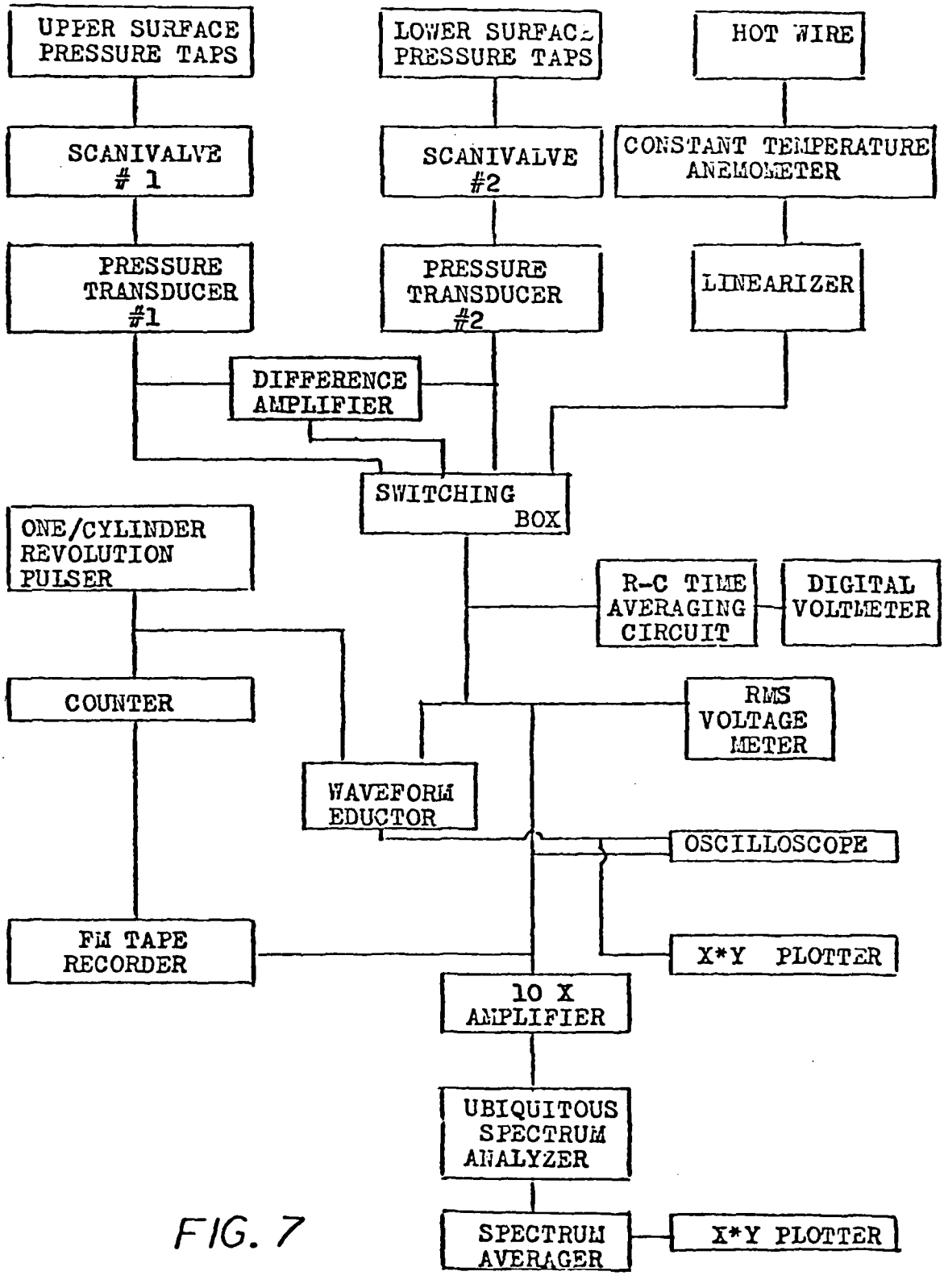

FIG. 7

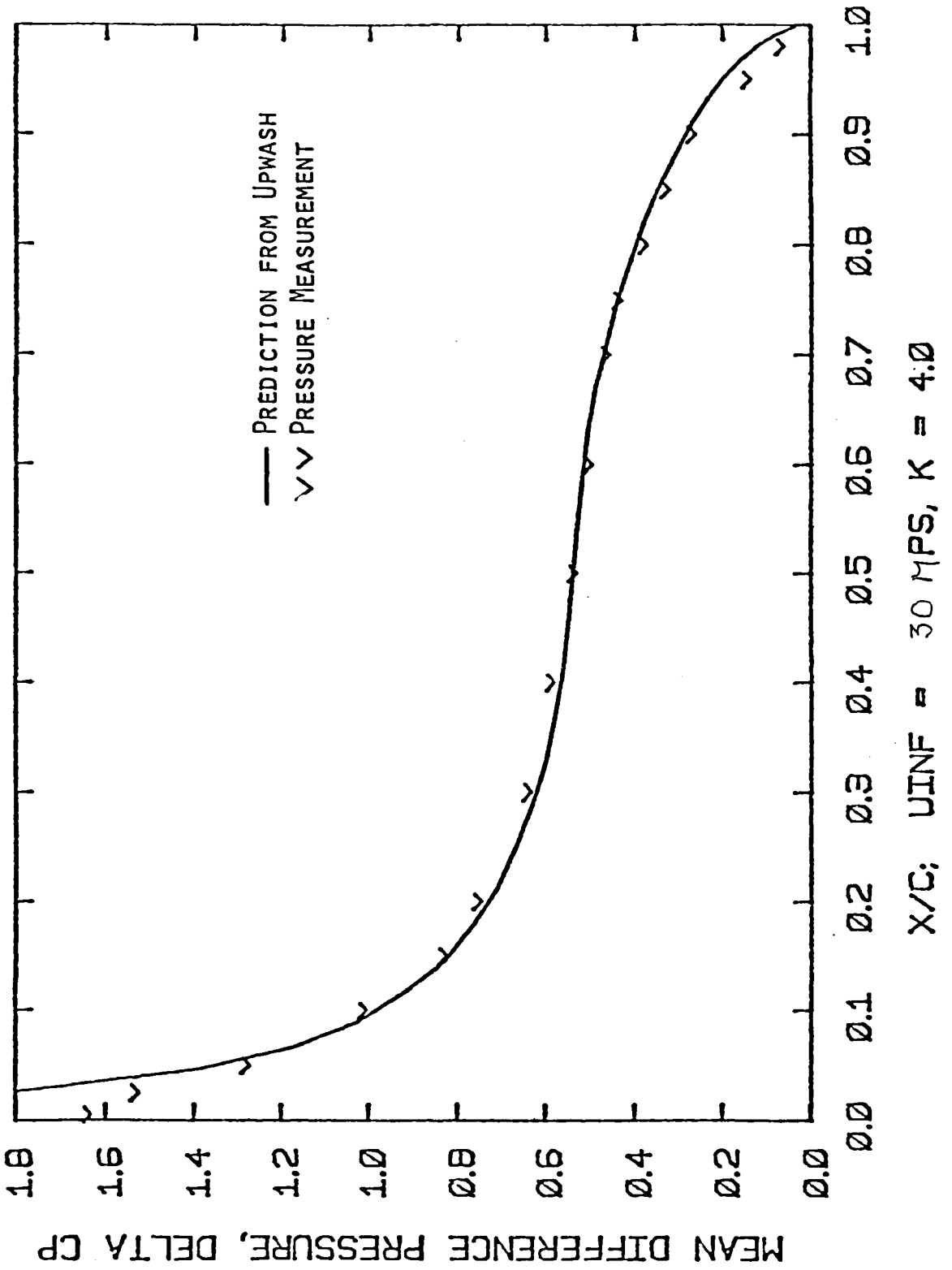
PREDICTION FROM UPWASH
PRESSURE MEASUREMENT
MEAN DIFFERENCE PRESSURE, DELTA CP
1.8
1.6
1.4
1.2
1.0
0.8
0.6
0.4
0.2
0.0
0.0
0.1
0.2
0.3
0.4
0.5
0.6
0.7
0.8
0.9
1.0
X/C; UINF = 30 MPS, K = 4.0

FIG. 8

FLUCTUATING DIFFERENCE PRESSURE AMPL.
0.30
0.25
0.20
0.15
0.10
0.05
0.00
0.0
0.1
0.2
0.3
0.4
0.5
0.6
0.7
0.8
0.9
1.0
X/C; UINF = 20 MPS, K = 2.0
PREDICTION FROM UPWASH
PRESSURE MEASUREMENT

FIG. 9

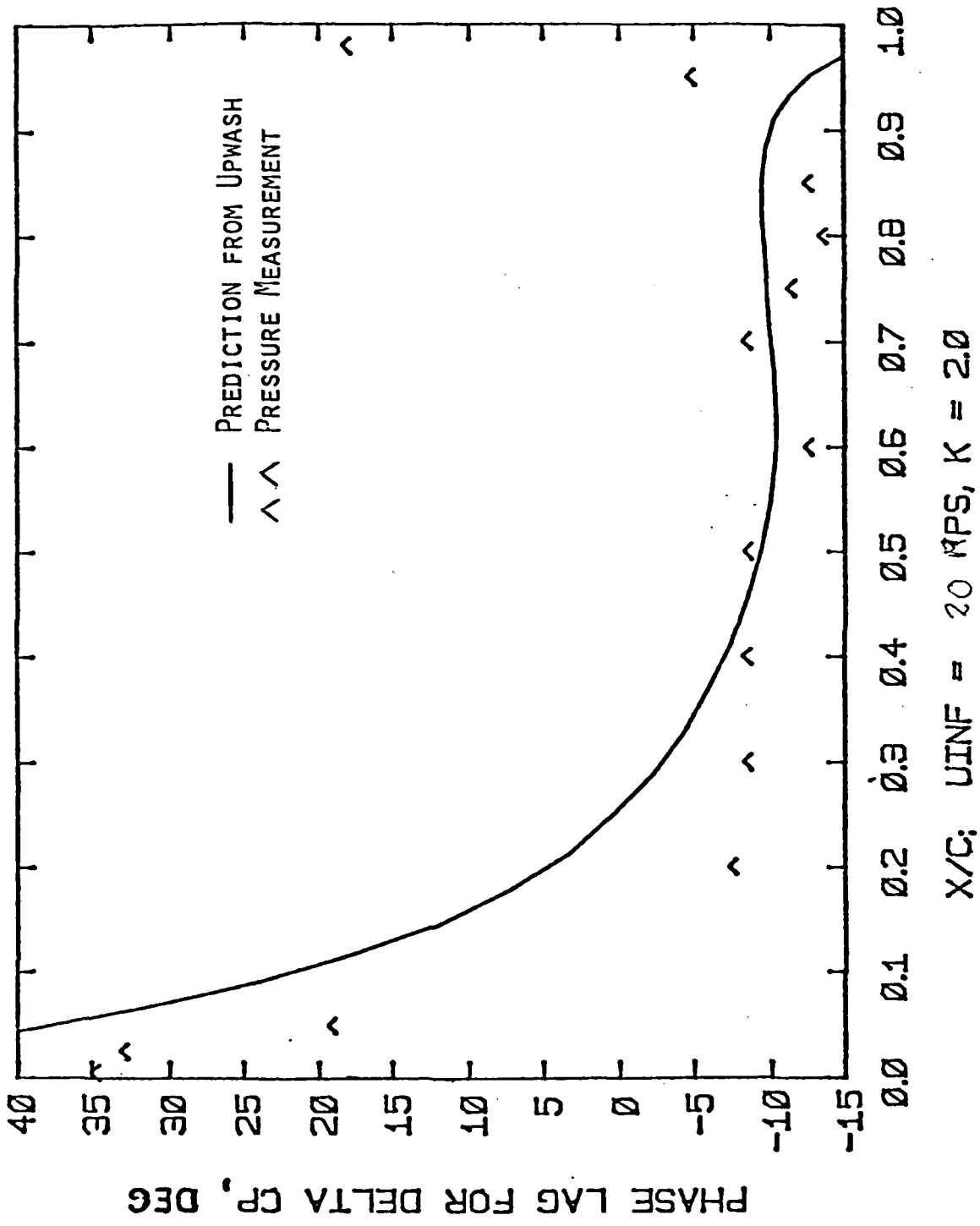
PREDICTION FROM UPWASH
PRESSURE MEASUREMENT
PHASE LAG FOR DELTA CP, DEG
40
35
30
25
20
15
10
5
0
-5
-10
-15
0.0
0.1
0.2
0.3
0.4
0.5
0.6
0.7
0.8
0.9
1.0
X/C; UINF = 20 MPS, K = 2.0

FIG. 10

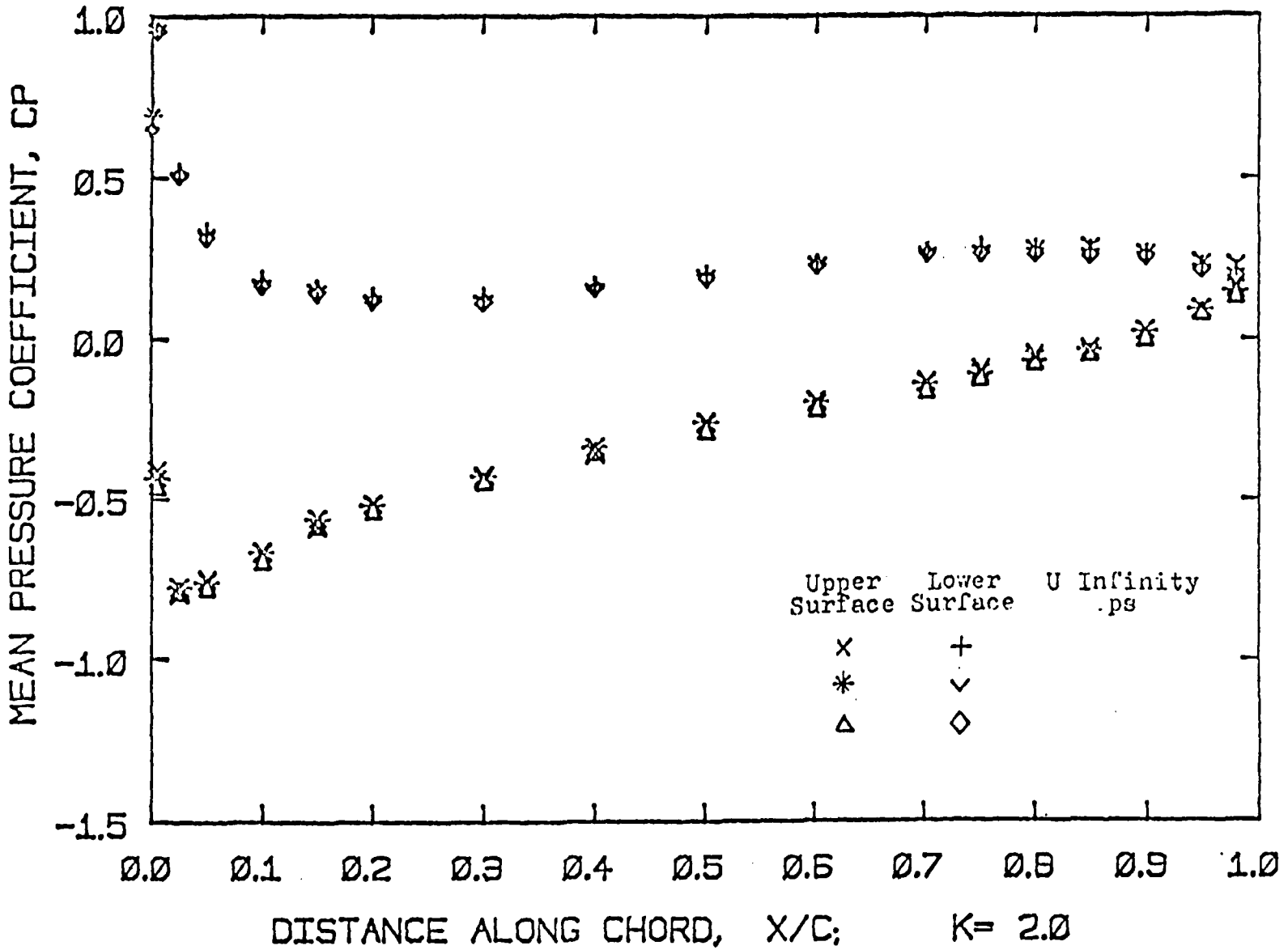
MEAN PRESSURE COEFFICIENT, CP
1.0
0.5
0.0
-0.5
-1.0
-1.5
0.0
0.1
0.2
0.3
0.4
0.5
0.6
0.7
0.8
0.9
1.0
DISTANCE ALONG CHORD, X/C;
K= 2.0
Upper Surface
Lower Surface
U Infinity .ps

FIG. 11

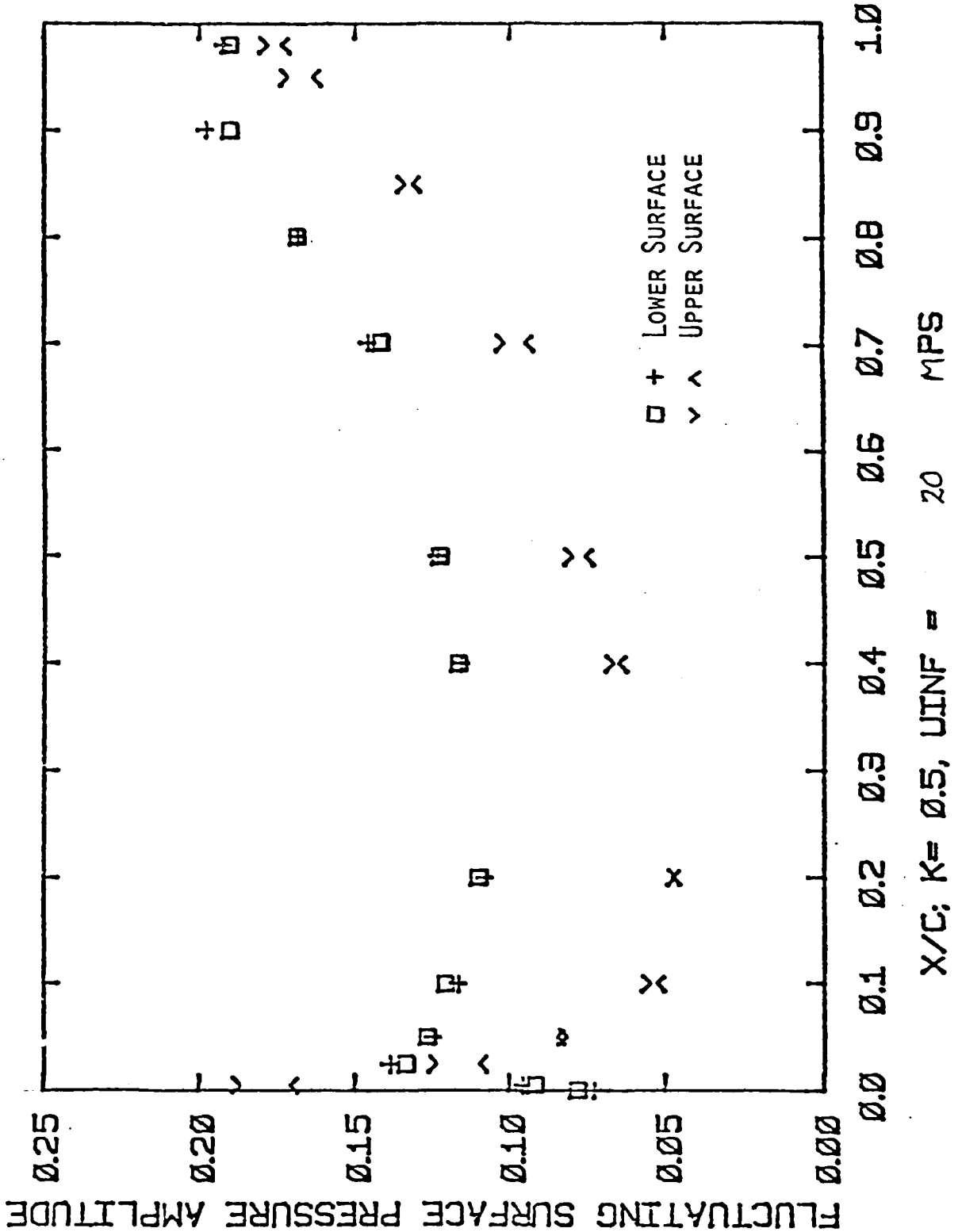
FLUCTUATING SURFACE PRESSURE AMPLITUDE
0.25
0.20
0.15
0.10
0.05
0.00
0.0
0.1
0.2
0.3
0.4
0.5
0.6
0.7
0.8
0.9
1.0
X/C; K= 0.5, UINF = 20 MPS
LOWER SURFACE
UPPER SURFACE

FIG. 12

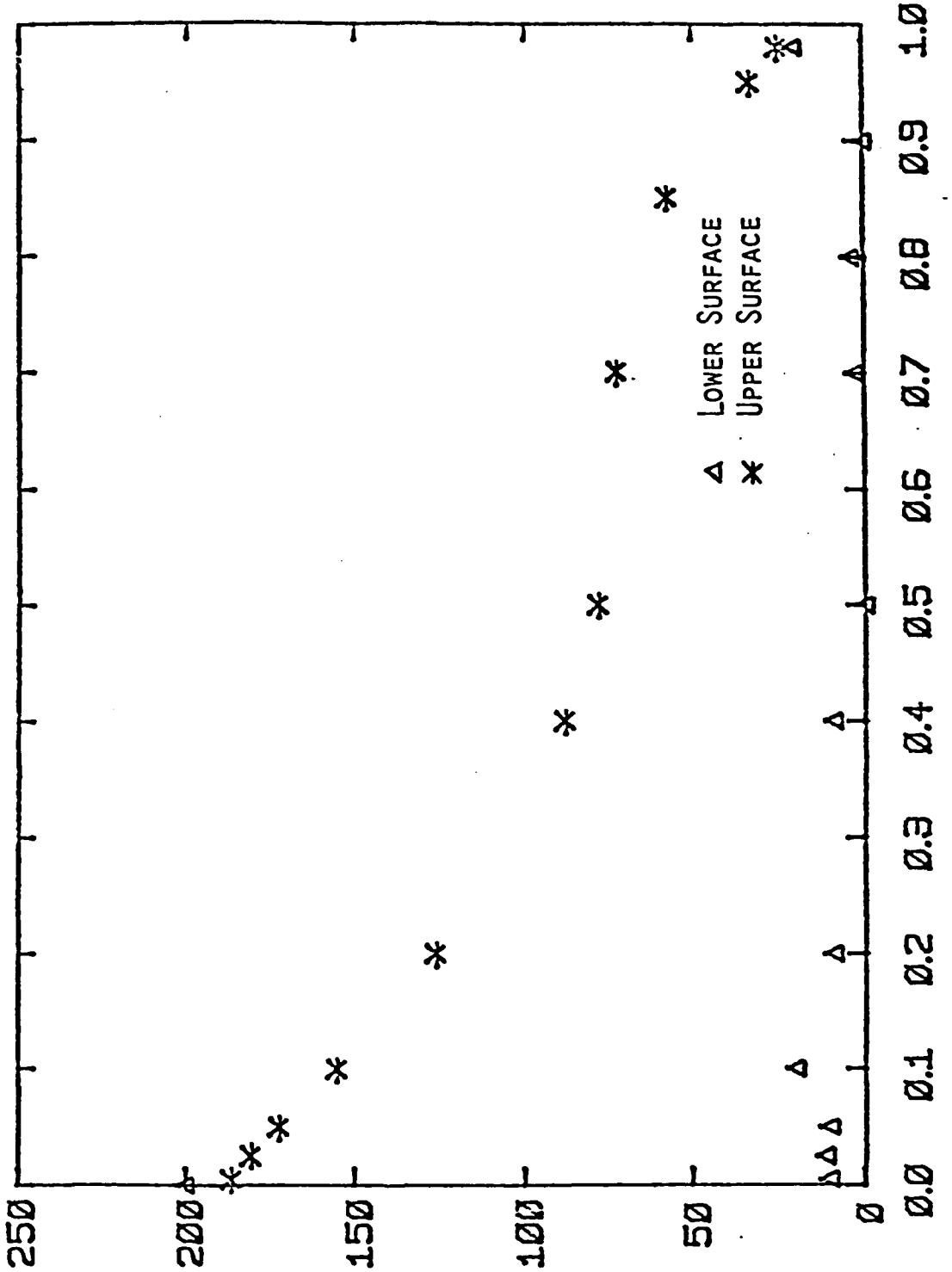
FLUCTUATING SURFACE PRESSURE PHASE LAG
250
200
150
100
50
0
0.0
0.1
0.2
0.3
0.4
0.5
0.6
0.7
0.8
0.9
1.0
X/C; K= 0.5, UINF = 20 MPS
LOWER SURFACE
UPPER SURFACE

FIG. 13

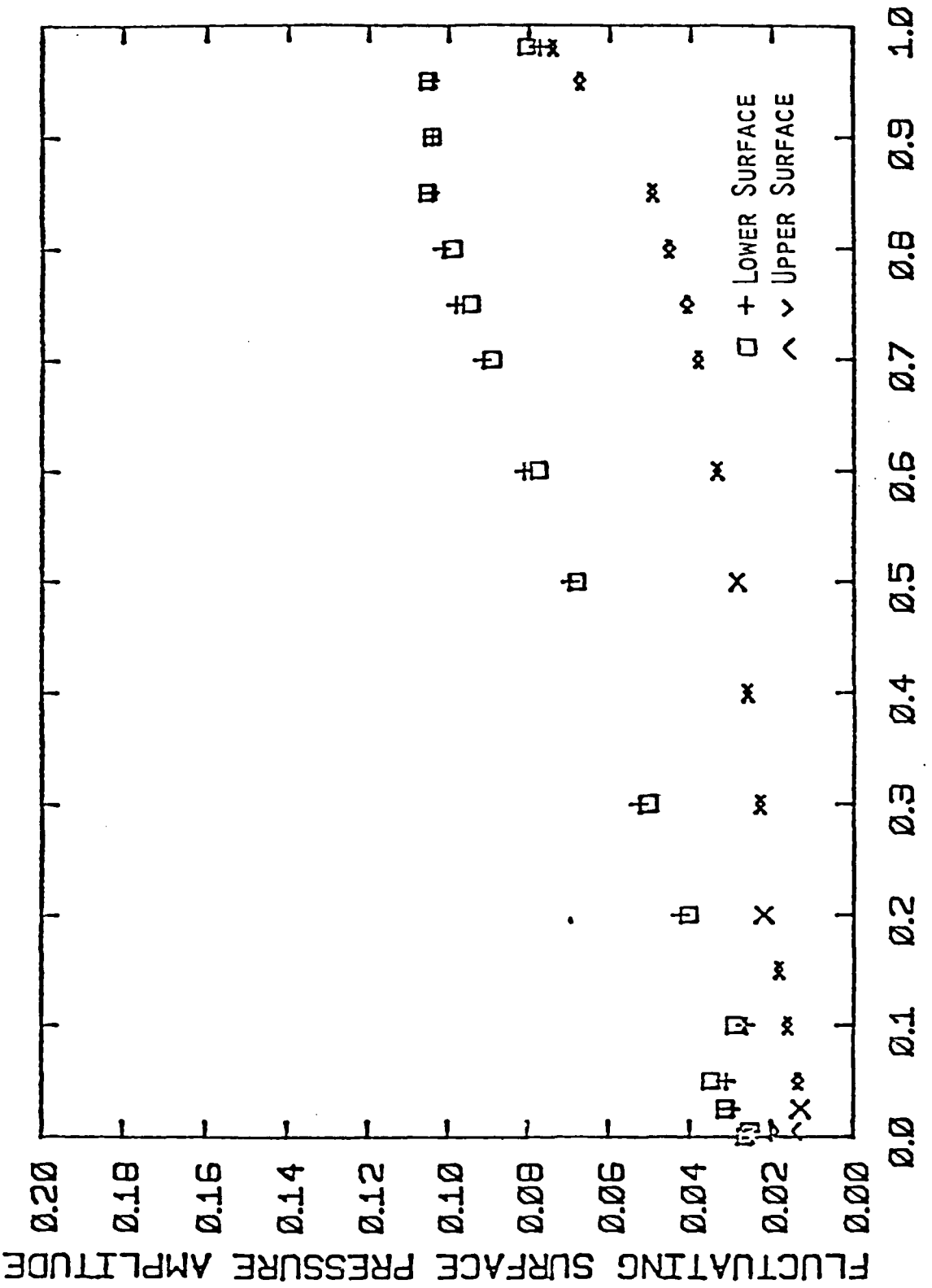
FLUCTUATING SURFACE PRESSURE AMPLITUDE
0.20
0.18
0.16
0.14
0.12
0.10
0.08
0.06
0.04
0.02
0.00
0.0
0.1
0.2
0.3
0.4
0.5
0.6
0.7
0.8
0.9
1.0
X/C; K= 4.0, UINF = 20 MPS
+ LOWER SURFACE
> UPPER SURFACE

FIG. 14

FLUCTUATING SURFACE PRESSURE PHASE, DEG
60
40
20
0
-20
-40
-60
0.0
0.1
0.2
0.3
0.4
0.5
0.6
0.7
0.8
0.9
1.0
X/C; K= 4.0, UINF = 20 MPS
LOWER SURFACE
UPPER SURFACE

FIG. 15

FLUCTUATING PRESSURE AMPLITUDE

UINF = 20 MPS X/C = 0.70

FIG. 16

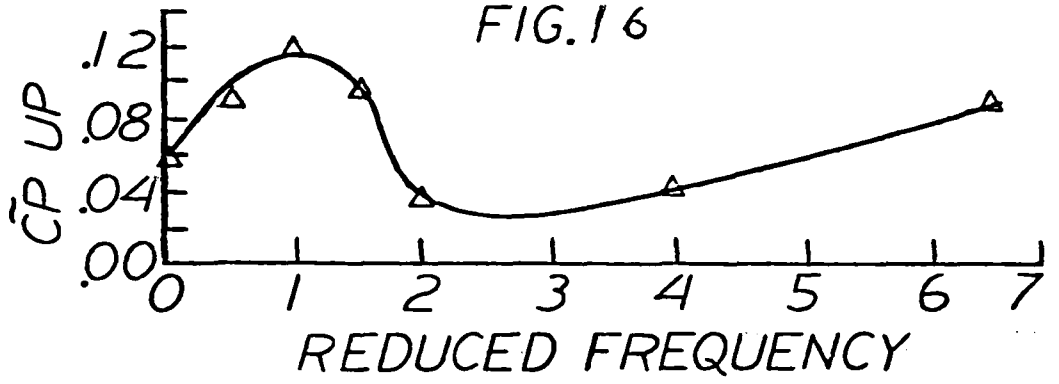

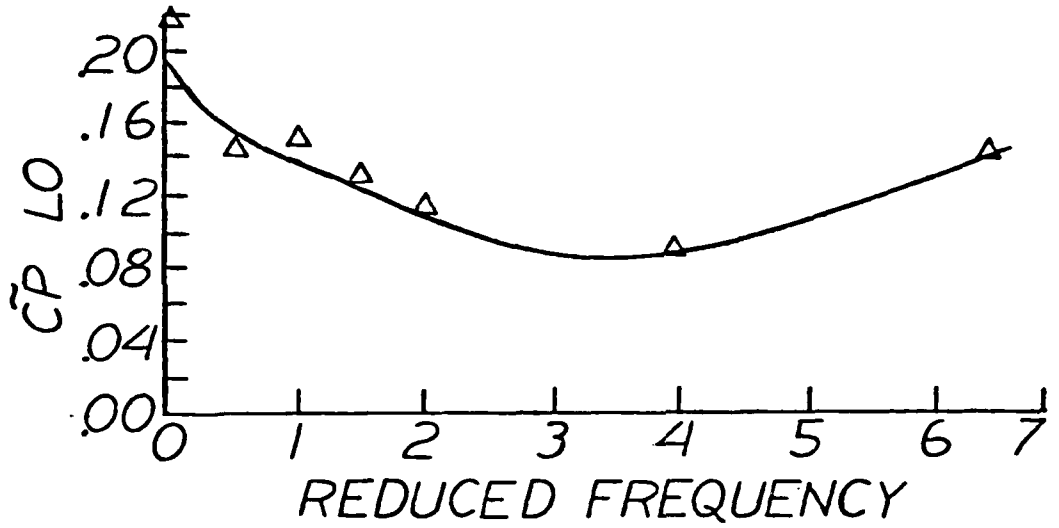

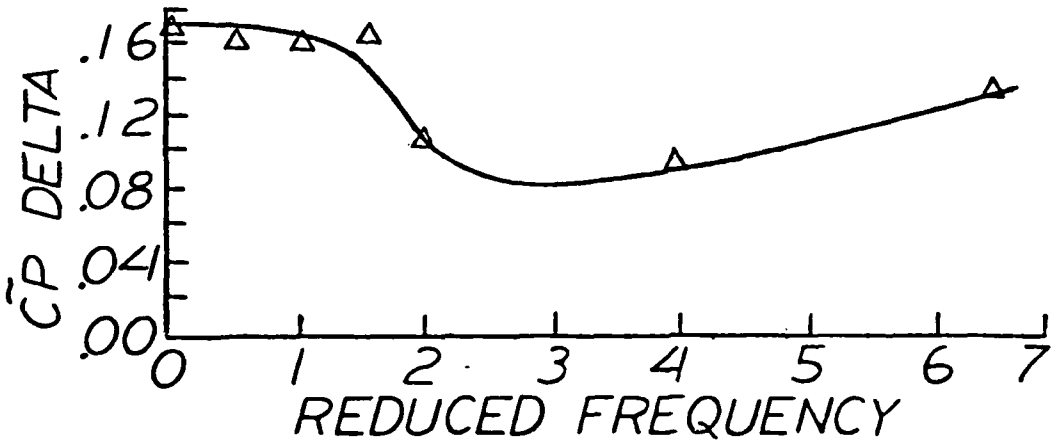

RMS DIFFERENCE PRESSURE NEAR AIRFOIL TRAILING EDGE

UINF (MPS) : +09, △20, ○30

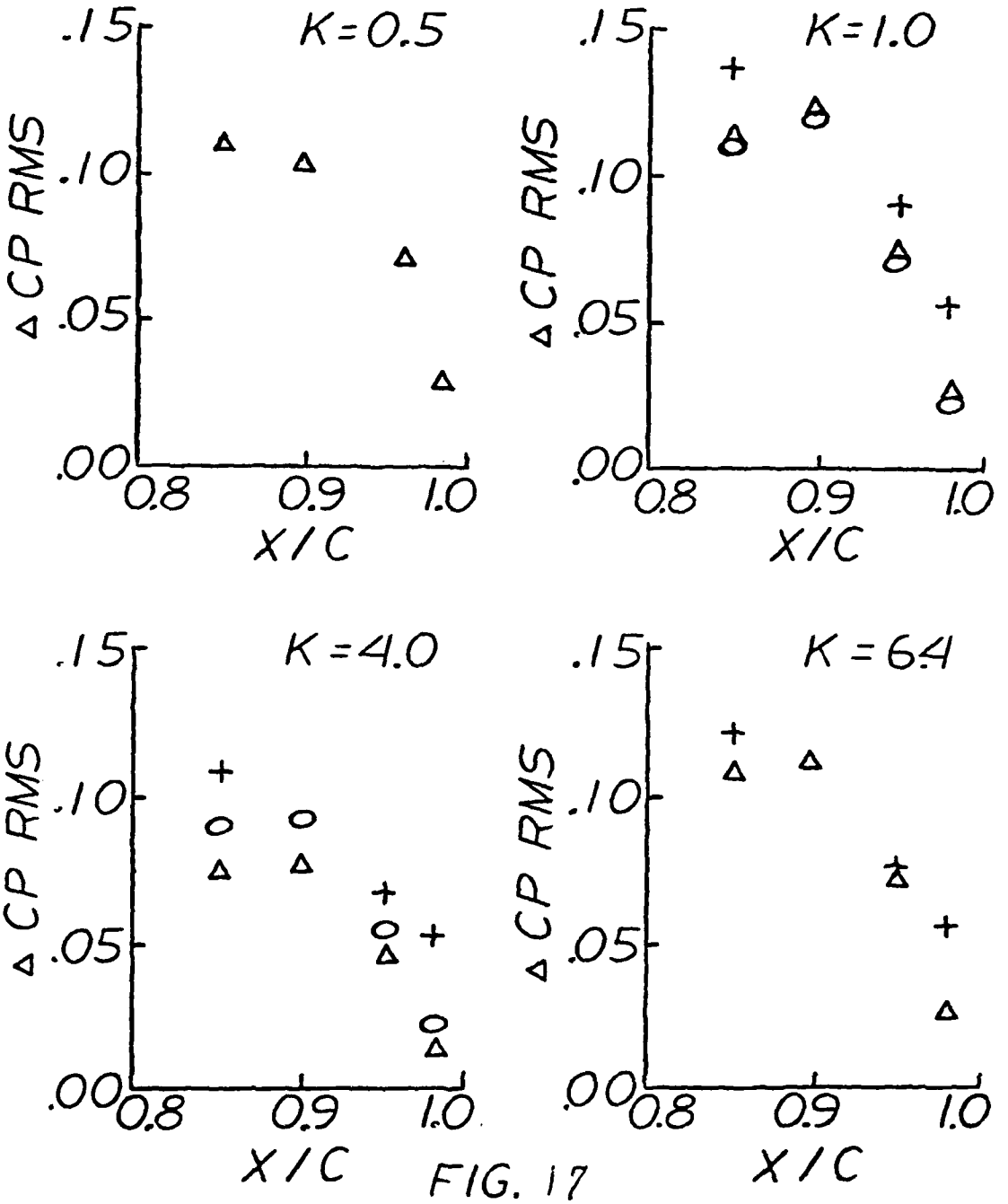

FIG. 17

CONFIGURATION FOR PRESSURE AND VELOCITY PROFILE STUDIES

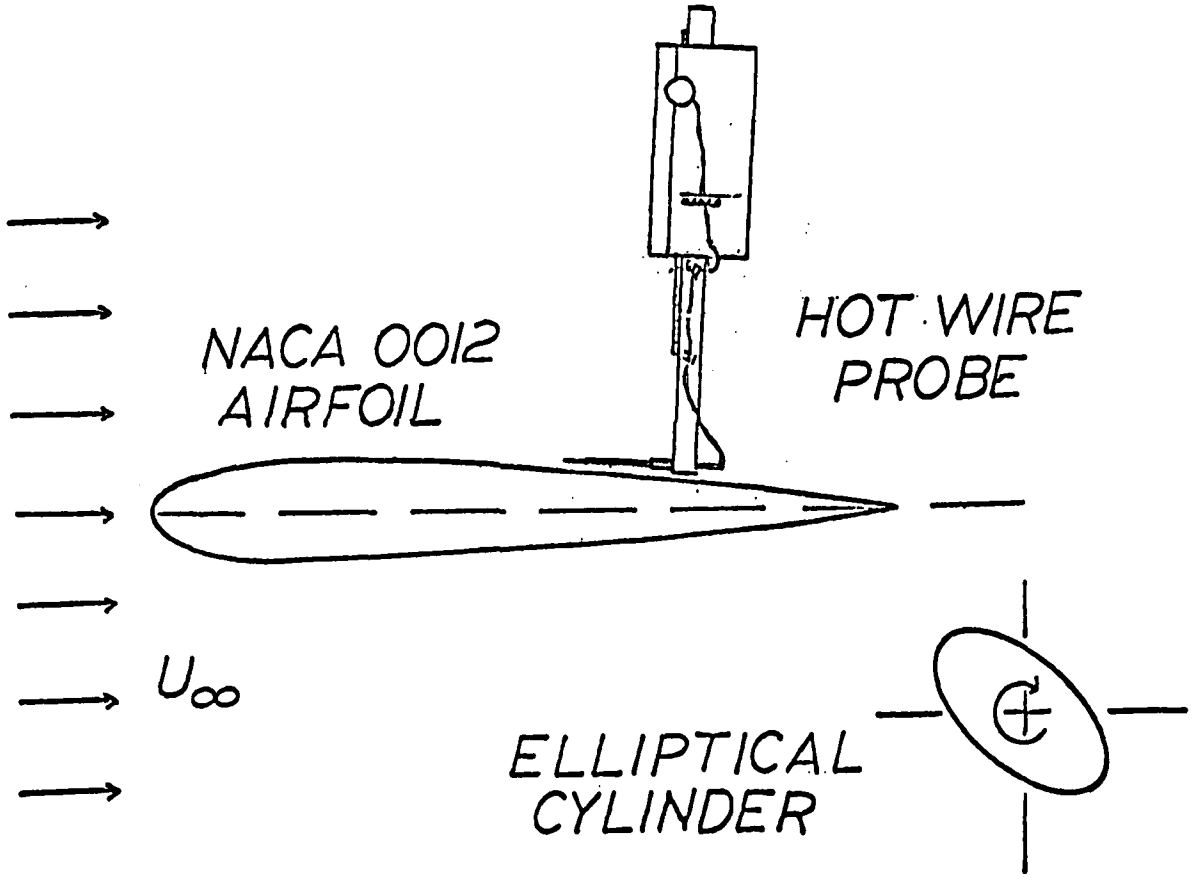

FIG. 18

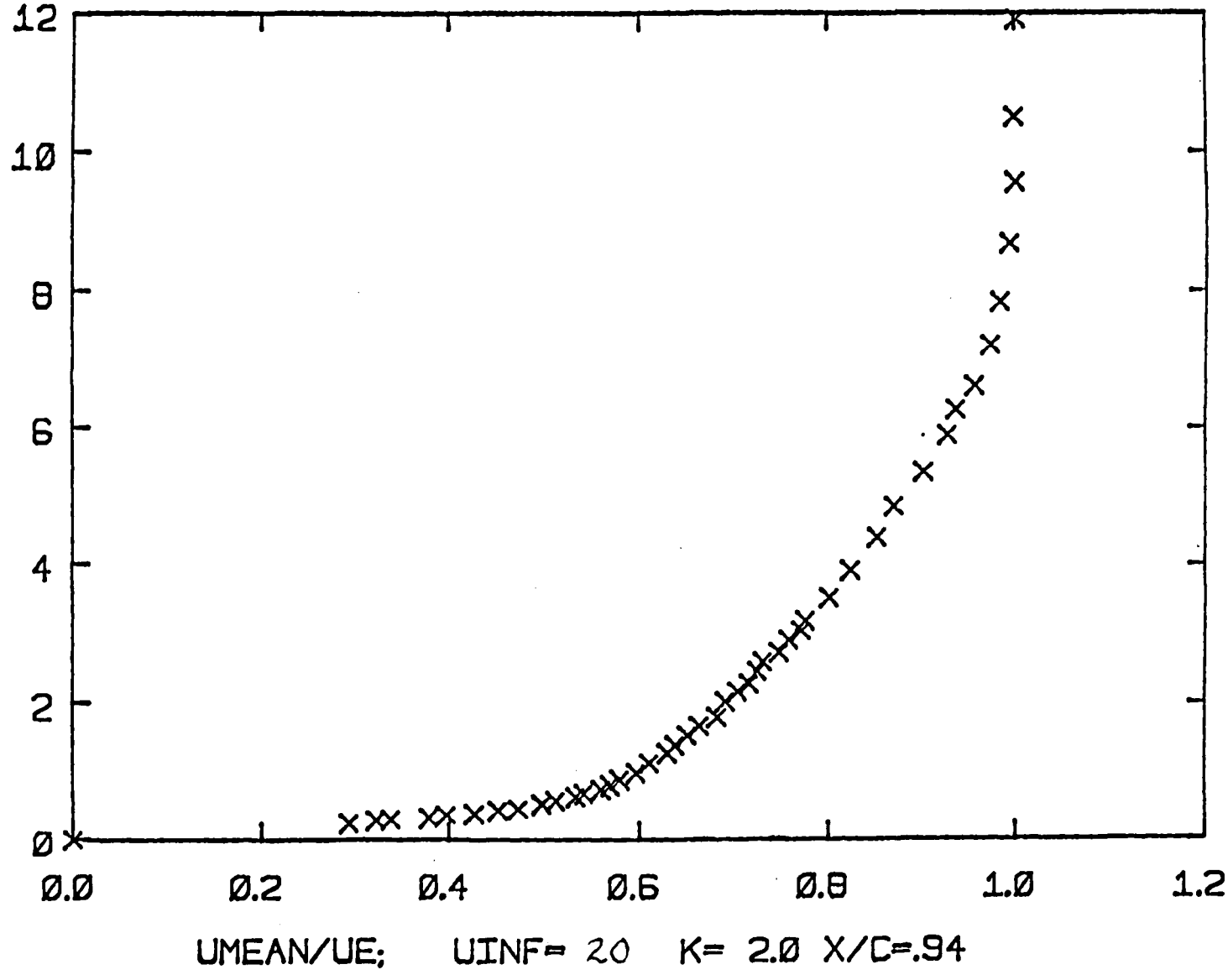

FIG. 19

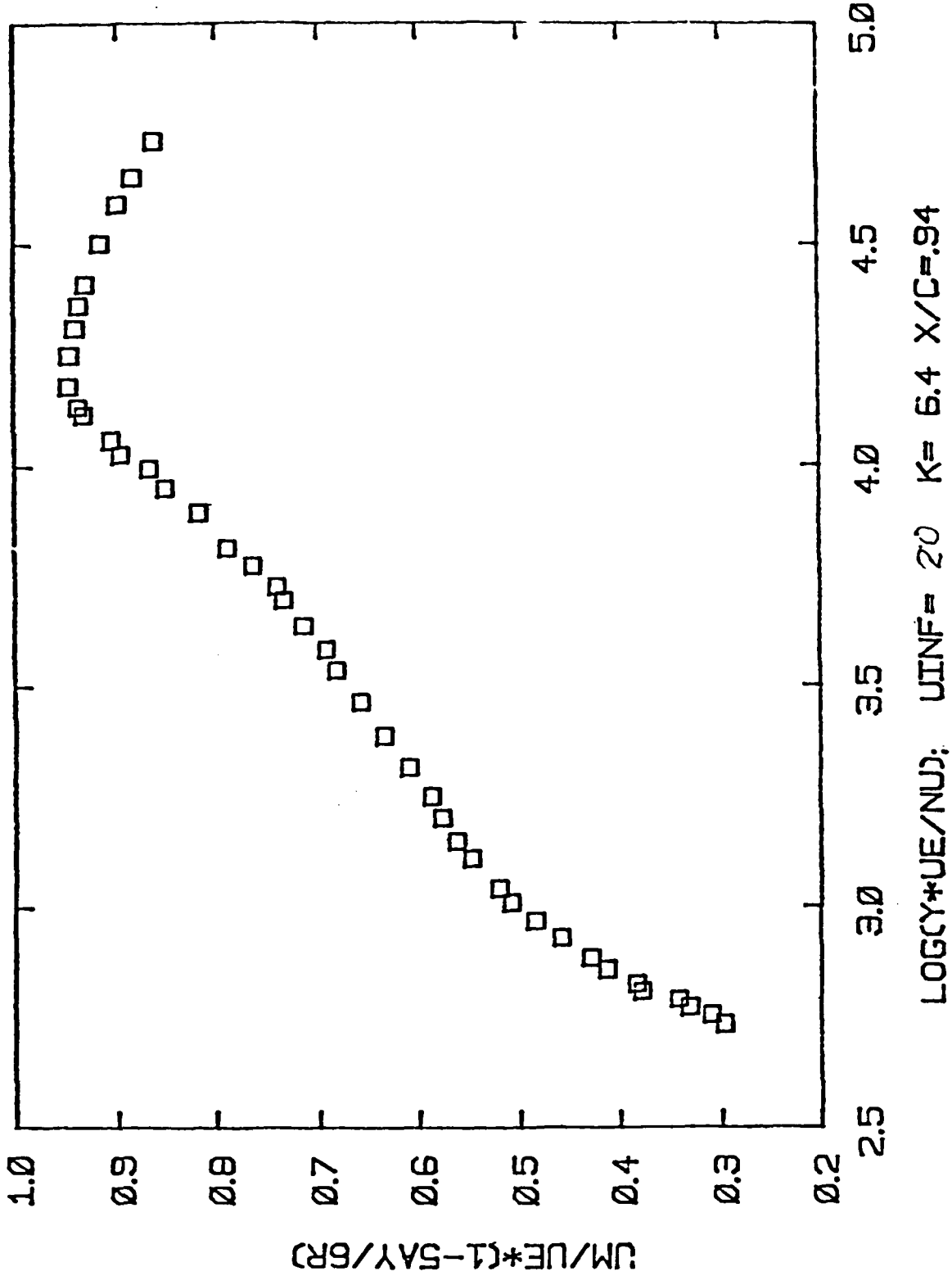
UM/UE*(1-SAY/6R)
1.0
0.9
0.8
0.7
0.6
0.5
0.4
0.3
0.2
LOG(Y*UE/NU); UINF= 20 K= 6.4 X/C=.94
2.5
3.0
3.5
4.0
4.5
5.0

FIG. 20

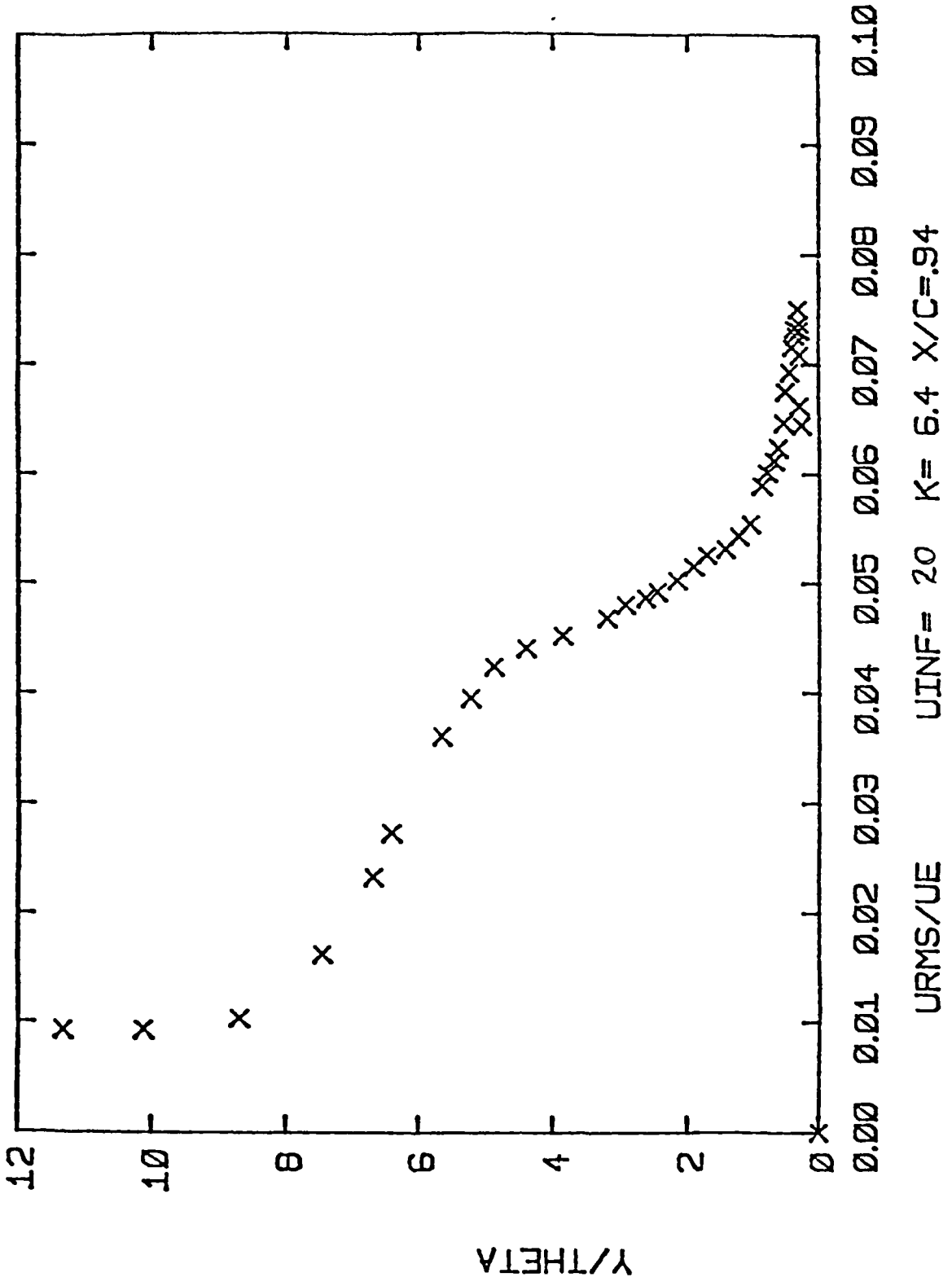
Y/THETA
12
10
8
6
4
2
0
0.00
0.01
0.02
0.03
0.04
0.05
0.06
0.07
0.08
0.09
0.10
URMS/UE
UINF= 20 K= 6.4 X/C=.94

FIG. 21

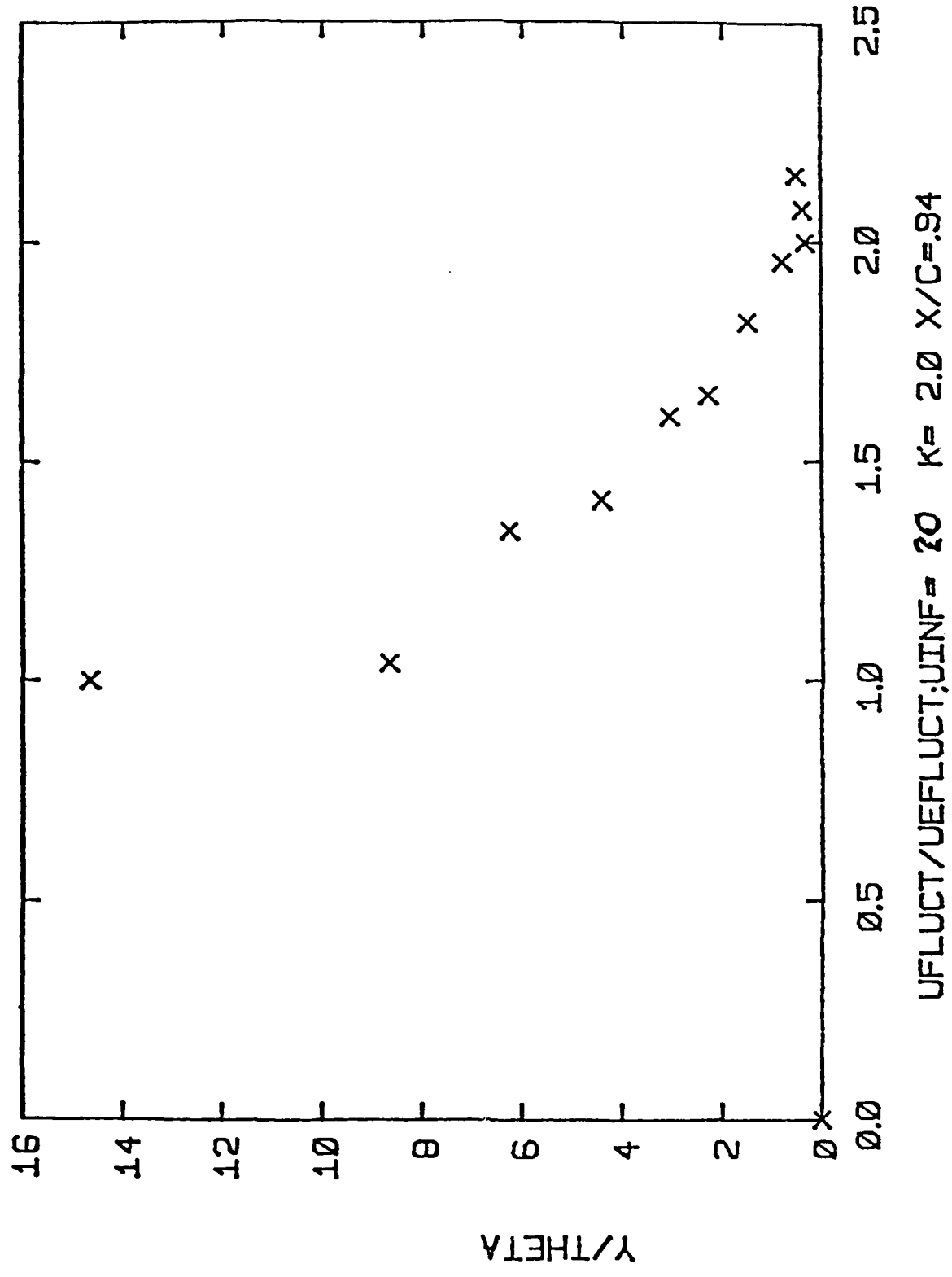
UFLUCT/UEFLUCT;UINF= 20 K= 2.0 X/C=.94
Y/THETA
0.0
0.5
1.0
1.5
2.0
2.5
0
2
4
6
8
10
12
14
16

FIG. 22

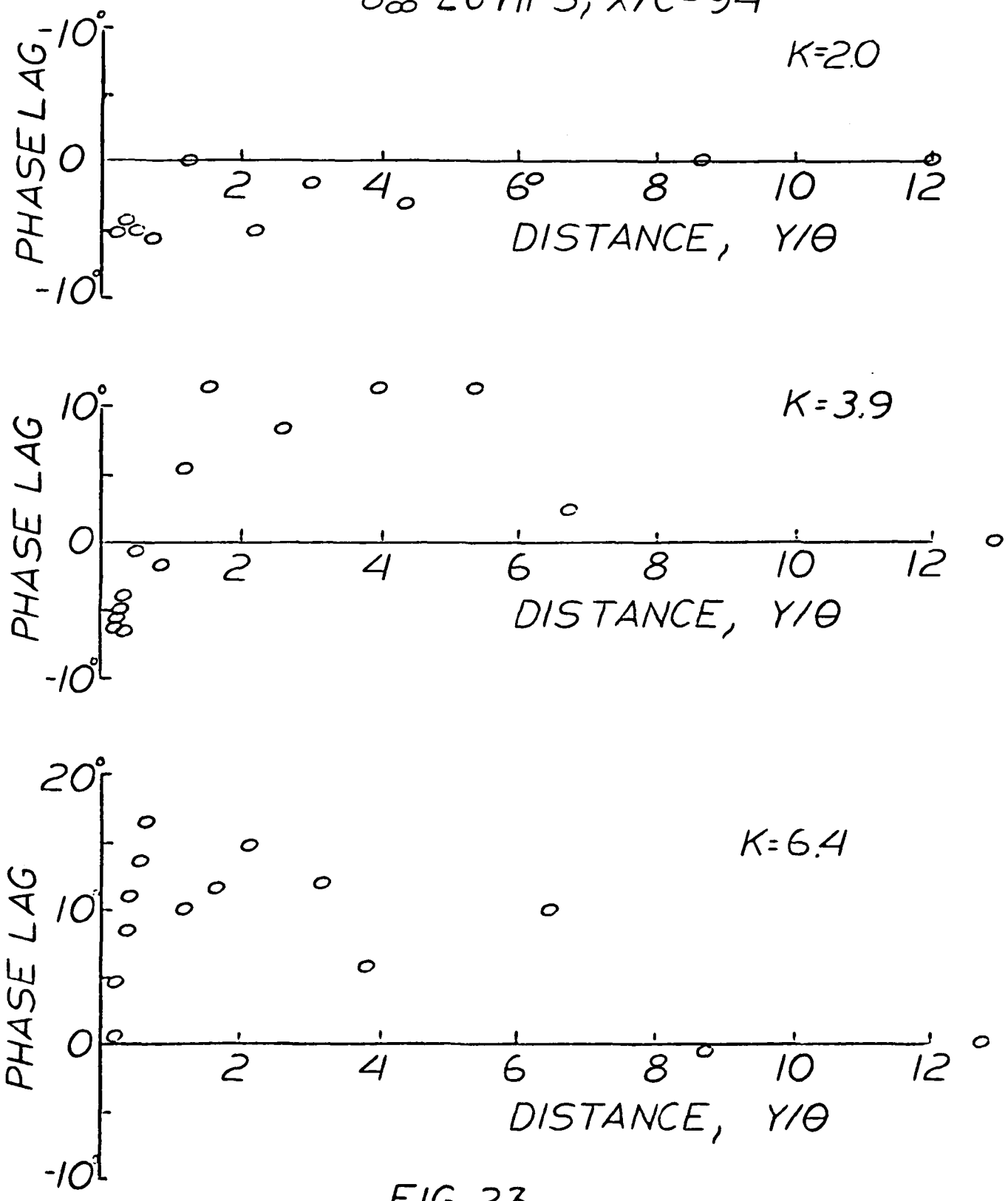
VELOCITY PHASE LAG
U_∞ = 20 MPS; X/C = 94
K=2.0
PHASE LAG
10°
0
-10°
2
4
6
8
10
12
DISTANCE, Y/θ
K=3.9
PHASE LAG
10°
0
-10°
2
4
6
8
10
12
DISTANCE, Y/θ
K=6.4
PHASE LAG
20°
10°
0
-10°
2
4
6
8
10
12
DISTANCE, Y/θ

FIG 23